Additive technology for pollutant control and efficient coal combustion.

Syed Sheraz Daood[*‡], *Marc Ottolini*[†], *Scott Taylor*[††], *Ola Ogunyinka*[‡], *Md. Moinul Hossain*[‡‡], *Gang Lu*[‡‡], *Yong Yan* [‡‡], *William Nimmo*[‡]

[‡] Energy Engineering Group, Energy 2050, Department of Mechanical Engineering, University of Sheffield, Sheffield, S10 2TN, UK.

[†] International Innovative Technologies Ltd, Unit 5, Queens Court, Third Avenue, Team Valley Trading Estate, Gateshead, NE11 0BU, UK.

[††] Sembcorp Utilities UK Ltd., Sembcorp UK headquarters, Wilton International, Middlesbrough, TS90 8WS, UK.

[‡‡] School of Engineering and Digital Arts, University of Kent, Canterbury, Kent CT2 7NT, UK.

KEYWORDS fuel additive, combustion efficiency, corrosion, flame temperature, NOx, particulate, slagging, fouling.

ABSTRACT High efficiency and low emissions from pf coal power stations has been the drive behind the development of present and future efficient coal combustion technologies. Upgrading coal, capturing CO_2, reducing emission of NOx, SO_2 and particulate matter, mitigating slagging, fouling and corrosion are the key initiatives behind these efficient coal technologies. This study focuses on a newly developed fuel additive (Silanite™) based efficient coal combustion technology, which addresses most of the aforementioned key points. Silanite™ a finely milled multi-oxide additive when mixed with the coal without the need to change the boiler installation has proven to increase the boiler efficiency, flame temperature with reduction in corrosion, NOx

and particulate matter (dust) emissions. The process has been developed through bench, pilot (100kW) and full scale (233 MW_{th}). The process has been found to have a number of beneficial effects that add up to a viable retrofit to existing power plant as demonstrated on the 233MW_{th} boiler tests (under BS EN 12952-15:2003 standard).

1. INTRODUCTION

The existing coal-fired power utility operators in the world are implementing ever stricter control regulations. For example, in Europe the European Commission's industrial emissions directive (IED); the USA's the clean power plan (TCPP) and environmental protection bureau china (EPBC). Successful agreements in Paris through recent the COPP21 Climate Change summit are leading the way to governments directing their economies toward lower carbon energy usage and power generation. However, in the interim period to decarbonisation, there is a need to continue to operate fossil fuel-fired power stations until a realistic balance of renewable technologies and nuclear power is achieved [1]. World-wide, coal-fired power generation has a 41% share of the total [2]; hence, there is a large opportunity for new technologies to impact on reducing emissions and increasing efficiency. Improvement of combustion efficiency with pollutants reduction (NOx, SO_2, particulate dust) has been proven with various coal conversion technologies including additive based technologies [3].

The additives broadly classified as organic and inorganic are presently used in power sector as catalysts [4]; however, in general, inorganic additives are widely applied due to the cost to benefit ratios [5-6]. Recently, many studies have been focused on the utilization of fuel additives to improve combustion and reduce pollutants on the bench to small pilot scales [7-14]. The use of these fuel additives economically sourced or formulated could be beneficial to address the

following problematic issues associated with coal combustion; 1-emission reduction (NO_x, SO_2, CO_2, CO and dust), 2-fly ash improvement (reducing unburnt carbon and the concentration of challenging ash species, increasing the melting points- ash fusion temperatures and particle size distribution), 3-combustion efficiency improvement (fuel savings, heat release and temperature gain), 4- dust emission reduction- post electrostatic precipitator, 5- resistance towards fireside corrosion.

For many power plant operators the improved thermal combustion efficiency and the implications for reductions in fuel consumption and emissions is likely to be highly significant factors, but for others, the ability to improve the quality of fly ash for re-sale into construction sector applications and resistance towards corrosion are likely to be priorities. Whatever the motivation for power station owners in different parts of the world, the range of proven benefits associated with the Silanite™ fuel technology means that it is extremely well placed in providing specific solutions to the individual power station challenges.

This study focuses on understanding the effectiveness of a newly developed solid pulverised fuel additive (Silanite™) towards NOx reduction, particulate control, and secondary effects on ash fusibility, slagging and fouling and boiler tube corrosion. Studies are presented from a pilot scale (100 kWth) combustor to commercial scale (233MWth ~ 260-280 tons/h steam output) pulverized fuel boiler. Corrosion studies (1000hr operation) were performed in lab scale furnace test reactors.

2. METHODOLOGY

2.1. **Pilot Scale Test facility**. The combustion test facility (Figure 1a) utilized for the pilot scale tests comprised of 8 x 400 mm (ID) sections with a total of 4 m furnace height and has a down-firing configuration. The throat diameter of the burner is about 66 mm with an overall maximum designed fuel thermal input rating of about 100 kW_{th}. In-flame measurement of CO_2, O_2, NOx, SO_2 and CO and the exit flue measurements along with temperatures throughout the furnace are recorded through USB high-resolution data acquisition personal daqview modules (Iotech). Further details of the combustion test facility (CTF) have been presented in other studies [12-13, 15]. The loss in weight twin-screw feeder (Rospen) utilized for coal feeding can feed coal up to 15-20 kg/h, and a small vibratory feeder was used to inject fuel additive. The feeder for the additive was calibrated to feed up to approximately 6% by volume or 13% by weight fraction of the coal feed. The fly ash was separated from the flue gas by cyclone separator before emission. The collection efficiency of the cyclone separator is about 96% plus for particles above 10 microns.

The gas measurements were recorded using chemiluminescence (NOx), non-dispersive infrared (CO, CO_2) and paramagnetic (O_2) working principle based standard instruments. The collected fly ash samples were subjected to XRF, LOI, Ash fusibility analyses.

2.2. **Utility Boiler**. The utility boiler having the maximum operating steam flow on coal of 260-280 tons/h, whereas, the minimum steam flow is 170 tons/h was selected for the commercial scale testing program. The combustion chamber volume for the boiler is about 1185 m^3 having furnace dimensions of 29 m x 7.5 m x 7.6 m with 770 m^2 to be an effective furnace heating surface exposed to the radiant heat. The throat diameter for all burners is about 650

mm with a total of 12 burners placed in 3 landings at 2440 mm apart between centers. The pf coal is radially fed into the burners with dedicated separate central coolant core air system for heavy fuel oil burners and igniters. The flue gas is pulled through the air heater and electrostatic precipitator with the use of two induced draft fans. Each of the ball and ring type coal (Babcock type 6.3E9) mills are charged with about 9-10 ton/h of sub-bituminous type pulverized (pf) coal. The forced draft fans rated at about 60 m^3/s flow rate supply the combustion air to the boiler. The main steam output gets distributed to pressure manifolds, of which customers are supplied with HP and IP steam. The overall process flow diagram (Figure 1b) of the boiler has been earlier reported in a separate study [12]. Oil or gas fuels are generally used during the start-up of the boiler. The utility boiler did not have the steam air heater, steam reheaters, flue gas recirculation and circulating pump arrangements.

The Silanite™ fuel additive was stored in a silo potentially away from the main boiler infrastructure and can be blown directly into the loss on weight feeder connected to the coal feeder feeding to the coal mills. This injection method gives good control of mixing ratio between the pf and the fuel additive without causing downtime to the boiler. The fuel additive loss on weight feeder was set to feed in about 3.4% by volume or 6.8% by weight equivalent to the coal feed. The particle size distribution of the additive and UK-based utility coal along with proximate and ultimate analysis is presented in Table 1.

All the plant-related data operations have been controlled/logged by the Delta V control system. The collected samples of fly ash, bottom ash, pf coal, coal lumps from stockpile, coal mill rejects were analysed for ultimate, proximate, CV, loss on ignition (LOI), XRF and ash fusibility analyses, respectively. The thermal efficiency calculation for the boiler[11] was calculated as per the BS EN 12952-15:2003 standard (eq. 1-4).

$$\eta\,(N)B = \frac{Q_N}{Q_{(N)}Ztot} \tag{1}$$

$$Q_N = m_{ST}(h_{ST} - h_{FW)} + m_{SS}\,(h_{FW} - h_{SS)} \tag{2}$$

$$Q_{(N)\,Ztot} = m_F H_{(N)tot} + Q_{(N)Z} \tag{3}$$

$$Q_{(N)}\,Ztot = m_F\left[(H_{(N)} + C_F(t_F - t_r)) \Big/ \left[1 - \frac{\gamma_{Ash}\,(1-v)}{1-\gamma_{Ash}-\gamma_{H2O}}\left(\frac{u_{SL}}{1-u_{SL}}\eta_{SL} + \frac{u_{FA}}{1-u_{FA}}\eta_{FA}\right)\right] + \mu_A C_{pA}(t_A - t_r)\right] + P_M + P \tag{4}$$

The calibration of the plant's continuous emission monitoring (CEM) analysers, collection of the fuel-fly/bottom ash-mill reject- fly ash samples, steady loads on the mill/boiler, water quality control was maintained by the operational team of the plant.

2.3. **Corrosion test facility**. Secondary impact of the additive technology is of major interest in the overall assessment for commercialization. To this end, a number of studies were performed to determine any effect of deposits including additive on corrosion rates. The corrosion test facility (Figure 1c) utilized used for this study (comprised of 6 silicon carbide electrically heated elements transversely placed in the top half of the furnace. The heating elements can modulate the temperature of the heated chamber up to 1200^{o}C. A gas mixture skid supplied the humidified simulated combustion gas products (O_2: 3-4%, CO_2: 14-16%, HCl: 0.03-0.05%, SO_2: 0.13-0.15%, N_2: 75-78%, H_2O: 6-8%) inside the electrically heated chamber. The simulated gas mixture is supplied through a metered skid connected to dedicated gas bottle cylinders. Thermal mass flow controllers based on the heat conductivity

of fluids are used to control and determine the mass flow. These thermal mass flow meters were calibrated by the supplier for the specific gas concentrations. A slight negative pressure differential of about 0.05-0.09 mbar was maintained across the heated chamber of corrosion test facility by using a compressed air venture vacuum generator, due to low flow rates. The exit flue gas mixture was scrubbed through a frequently replaced solution of NaOH (0.5 M).

T22 ferritic steel alloy (Cr: 2.25%, Mo: 1%) sample coupons after surface preparation [16-17] and coating with the coal fly ash and fuel additive (Silanite™) mixed fly ash were placed inside the crucibles positioned in the heated compartment. The specimen coupons were all prepared in the same way by polishing to a uniform surface roughness using P120, P 240, P 280, P400 and P1200 silicon carbide paper for later dry polishing with diamond paste. 24 point measurements were taken across the whole surface of the polished coupons using a Mitutoyo +/- 2-micron accuracy micrometer to acquire an average thickness of coupons. Ethanol was added to the fly ash to facilitate a uniform stable coat (ethanol would be dried off at room temperature). The coatings were applied using a fine brush for even coatings. These coupons were conditioned at 200^{o}C in the furnace for 2 hours after coating each specimen with the collected ash samples (Table 1). These coupons later were shifted to crucibles for weighing and positioned inside the furnace exposed to the simulated combustion environment maintained at 560^{o}C for 1000hrs. The coated coupons are placed on top of the ceramic plate and covered with an inverted ceramic liner with gas tight inlet and outlet connections. The heated compartment comprised of a base Inconel plate which is protected by a ceramic plate, the peripheries of Inconel plate were sealed with high-temperature grade silica powder.

The coupons were later analysed by accurate measurement for the metal loss. This was achieved by removing any deposited scale after 1000-hour exposure to reach to the bare metal and again 24 point measurements at the same positions were taken to compare the difference in measurements between pre and post testing. These coupons were prepared in duplicates and the reported findings are based on the average of the results.

3. RESULTS AND DISCUSSION

The following section details the overall findings associated with the technology. The evaluated parameters alongside the discussions on array of tests performed on all of the aforementioned setups starts from the commercial to the pilot scale tests.

3.1. **BS EN 12952-15:2003- boiler commercial test.** A detailed breakdown of the test protocol followed during the test is shown in Table 2. The reported findings are associated with the full scale boiler test incorporating the overall impact on the efficiency, emissions, flame temperature, LOI, dust concentration, particle size distribution (PSD), slagging and fouling propensities and ash fusibility temperatures.

3.1.1. The commercial full scale 8-hour long test results on the 260 tons/h, as per the BS EN 12952-15: 2003 resulted in a net gain of about 1.05% increase in the boiler efficiency (eq 1-4, Table 3). An overall 8 hours of steady state levels were maintained by keeping the loads on the coal mill- downstream high -intermediate pressure steam manifolds under unaltered conditions. The costs savings on the fuel input for maintained fixed output from the plant could also be regarded as an additional CO_2 reduction (due to reduced parasitic load on coal mills / air heaters and other ancillary equipment because of 1.05% less coal consumption).

3.1.2. A net 8.4% reduction in NOx has been found compared to coal baseline with 3.4% by vol. (i.e. 6.8% wt.) the addition of fuel additive (Figure 2a). NOx reduction in line with predictions (trials done earlier on 100kWth pilot-scale combustion test facility and a 45min trial on 280tons/h steam-producing boiler [12]- Figure 2b-c). The CEM of NOx emission (uncorrected) at the three different locations of the boiler for the baseline tests were reported as 195, 201 and 382 mg/Nm^3. They were compared at the same locations as 185, 167 and 357 mg/Nm^3 respectively when firing with 3.4% vol. additive injection. Then these measurements were corrected for the standard oxygen concentration of 6% (dry basis) along with plant recommended CEM instrument correction factors. The corrected NOx value for the baseline of 564 mg/Nm^3 was compared with NOx value obtained during the additive injection of 517 mg/Nm^3. The trial results have proven a net 8.4% reduction with the addition of 3.4% by vol. additive. This is in line with the earlier trials on both pilot and full-scale combustion test facility and boiler, respectively. CEMs normally get purged after every 12 hours; hence around 14:10 the instruments got purged with air as evident from Figure 2a. The scatter of the points in the initial coal baseline when calculated as standard deviation was 21.6 compared to 25.57 for coal and coal with additive, respectively. Post additive injection, the downstream demand of the steam increased resulting in the increase of the coal mill loads (i.e. after 15:00). Hence the higher fuel to air ratio (i.e. fuel rich condition) produced lower NOx levels (Figure 2a).

3.1.3. The monitoring and characterisation of the coal / coal-additive flames on the viewing port of landing B of the boiler was also undertaken. The flame measurement was recorded for 8-10 minutes with the flame videos taken at a frame rate of 25 fps (frames per second) for observation purposes. The camera of the system was kept at the same settings (iris and

exposure time) during the test. It was found that no detrimental effect on the flame temperature was recorded with the addition of the additive. In fact, 11^{o}C increase in the average flame temperature (Figure 3a) was observed with the additive injections in comparison to coal baseline (1494^{o}C). Each condition used to compute the average flame temperature included 150 to 200 simultaneous images. Temperature distribution of flames was computed using flame images averaged over 20 simultaneous imaged based on the two colour method [ref]. Moreover, the power spectral density (PSD) of the flame signal (Figure 3c) were computed based on the average grey-level of each image from the video images recorded using the high speed mode (200 fps) of the camera over about 2 minutes [ref]. The oscillation frequency of the flame with and without additive was obtained using the weighted PSD of the flame signal. It remained in the range of 27-30Hz suggestive of no adverse effect of the additive on flame stability. The effect of the additive on the flame area was examined by applying an appropriate threshold to the segmented luminous region of each image; this was later normalized to the image size. These normalized flame areas were recorded to be in the range of 28% to 30% for coal and coal + Silanite™ baselines (Figure 3c).

3.1.4. The fly ash samples were taken from the fly ash hoppers post Electrostatic precipitators (ESPs). The hoppers were emptied before and after steady state conditions by a dedicated fly ash recovery vacuum system, this allowed collection of the representative coal fly ash samples. The representative samples were stored in air tight clearly marked barrels for further analysis. Barrels numbered 1 to 11 were designated for coal fly ash collection; whereas barrels number 13 to 23 were used to collect fly ash with the additive. Later two more samples were taken post additive injection in Barrels 25-26. The collected samples were later analysed as per ASTM D7348 to determine the loss on ignition values. The calculation of

loss on ignition (eq 5) from the single step procedure used is as follows:

$$LOI = [(W-B)/W]*100 \quad (5)$$

Where W = mass of test specimen used, g, and B = mass of test specimen after heating at 950°C, g. The LOI values for coal fly ash samples gave a range from 14.5% to 15.7% for barrels from 1 to 11. This averages to be about 15% -coal fly ash baseline. On the other hand, a range of 8.1% to 9.8% was determined for coal + 6.8% Silanite fly ash samples, averaging to be about 8.6%. Figure 4 shows the LOI data points respective to samples collected from 1st, 2nd or 3rd fly ash hoppers post ESPs. The scatter of the points in the initial coal baseline when calculated as standard deviation was 2.8 compared to 3 for coal + 6.8% Silanite. A net 42.7% reduction in LOI was observed with the injection of the fuel additive. In all cases, LOI in fly ash show the reduction after injecting the fuel additive.

3.1.5. Dust concentration post electrostatic precipitators (Figure 5) have been reduced by approximately 18% with the Silanite™ injection indicating better performance of ESPs. The reductions in the unburned carbon present in the fly ash and the conductive properties of the oxides of iron (in the additive) have resulted in the reduction of dust concentration emitted in the stack. Silanite™ injection delivers a positive impact on the chemical composition of fly ash, particle size and the resistivity- crucial parameters for improvement of the electrostatic precipitator performance. The recorded concentration of the dust post ESPs are tabulated in Table 4 and Figure 5 entails dust concentration plot for both 45 min- 8hr and 1hr trials carried out on the same boiler along with the full-scale BS EN 12952 8h test. The scatter of the points in the initial coal baseline when calculated as standard deviation was again close to that of coal with Silanite™.

3.1.6. The Air Jet PSD analysis conducted on the coal – Sialnite™ fly ash samples collected during the 8h trial indicated 90% passing at 335 microns compared to 508 microns for the coal fly ash. It is also evident from Figure 6 that the coal - additive mixed fly ash is finer than compared to coal fly ash. This is mainly associated with the injection of the additive having d0.9 less than 34 microns compared to a typical coal having d0.9 less than 125microns. The fineness of the coal - Sialnite™ fly ash also qualifies it for EN450 (not more than 40% retained on the 45 microns sieve). The resultant coal fly ash with the injected Silanite™ is finer then coal fly ash.

3.1.7. The slagging and fouling propensities calculations from the full scale 8h trial has indicated no detrimental impact on the slagging and fouling propensities. This is due to the combined concentration of the oxides of iron, aluminium and silica. Table 5 entails the findings of XRF analysis with the major and minor elemental oxide concentrations present in the fly ash and Sialnite™ respectively. These concentrations have been utilised to calculate the fouling and slagging indices as per the equation 6-7.

Fouling Indices [18-19] $= \mathrm{Fu} = \left(\frac{\mathrm{B}}{\mathrm{A}}\right)\left(\mathrm{Na_2O} + \mathrm{K_2O}\right)$

Fu $\leq$ 0.6 low fouling inclination
Fu = 0.6-40 medium
Fu $\geq$ 40 extremely high (6)

Slagging Indices [18-19] $= \mathrm{Rs} = \left(\frac{\mathrm{B}}{\mathrm{A}}\right)\mathrm{S}^{\mathrm{d}}$

$\left(\frac{\mathrm{B}}{\mathrm{A}}\right) = \left(\frac{\mathrm{Fe_2O_3} + \mathrm{CaO} + \mathrm{MgO} + \mathrm{Na_2O} + \mathrm{K_2O}}{\mathrm{SiO_2} + \mathrm{Al_2O_3} + \mathrm{TiO_2}}\right)$ in dry fuel

Rs < 0.6 low slagging Inclination
Rs = 0.6-2.0 medium
Rs = 2.0-2.6 high
Rs > 2.6 extremely high (7)

3.1.8. The samples collected as part of 8 hour trial were subjected to ash fusibility as per BS ISO 540:2008. The ash fusibility temperatures were determined using Carbolite digital CAF-8. The samples tested were analysed on as received basis. Ash samples were mixed with an adhesive dextrin solution to prepare a paste mixture. The cylindrical mould was first quoted

with a thin layer of petroleum jelly. The mould was uniformly and completely filled with the prepared paste of ash so that edges of cylindrical test pieces are sharp. Upon visual drying, the specimens are removed from the mould on its support to dry overnight. Two identical cylindrical samples were prepared for the same sample for repeatability purposes and placed on support next to each other. The test pieces are visually examined with the camera after loading in Carbolite digital furnace. The slow gradual increase in temperature to about 815^{o}C caused the removal of any organic matter @ 10^{o}C/min. The specimen and recording of the shapes at intervals of temperature change not greater than 10^{o}C were recorded until the flow temperature of the specimen has been attained. The fusibility temperatures observed during the analysis are defined as follows; the deformation temperature at which the first sign of rounding, due to melting, of the tip or edges of the test piece, occur. Sphere temperature is at which the edges of the test pieces become completely round with the height remaining unchanged. Hemisphere temperature at which test piece forms approximately a hemisphere (height becomes equal to half of the base diameter). Flow temperature at which the ash melt spread out over the supporting tile in layer (height of which is one-third of the height of the test piece at the hemisphere temperature). The analysis of the samples did not indicate difference in the initial deformation and sphere temperature of coal fly ash samples with and without additive, however, hemisphere and flow temperature were observed to be higher for coal- Silanite™ fly ash compared to the simple coal fly ash (Table 6). This is an indication of the formation of high temperature eutectic mixtures of fly ash with the lower slagging propensity. It is evident from the data that a suppression of about 10^{o}C-30^{o}C has been observed in the flow temperature with the additive combined coal fly ash samples. Similarly a 10^{o}C-20^{o}C increase in hemisphere temperature was observed for additive combined coal fly

ash samples. During the ash fusibility tests it was also verified that the coal fly ash samples exhibited greater shrinkage rate compared to the Sialnite™ -coal fly ash samples. The shrinkage of the samples with the temperature can be observed in a sequential comparison of the images obtained. The image analysis of revealed that there was an overall 53.26% reduction in the image area of coal fly ash sample compared to 46.02% reduction in the image area for coal with the additive fly ash sample. The approach has been applied to other samples endorsing relatively lesser shrinkage compared to the simple coal fly ash samples. These remarkable differences of shrinkage rates are attributed to sintering characterisation of the fly ash. Hence from the analysis of the images, it has been verified that coal with additive fly ashes has relatively lesser tendency to sinter compared to the simple coal fly ash because of lesser shrinkage rates.

3.2. **100kW$_{th}$ Furnace test results.** To establish the influence of Silanite™ towards NO reduction and to endorse the earlier reported findings [12-13, 20-22] of catalytic reduction of NO by combustion intermediate i.e. CO over the surface of oxides of iron, radial and axial profile measurements were recorded from the pilot scale 100kW$_{th}$ furnace combustion tests. Convincing evidence specifies better results towards de-NOx using low-cost iron oxides in conjunction with other commercially available technologies i.e. reburning, advance reburning, selective non-catalytic reduction[22-24]. The inflame measurement of CO at the module 1 (port 1) position confirmed higher concentrations with Silanite™ (Figure 8a) compared to coal baseline measurement at the same location. However, later at the module 2 (port 2) location, the values were recorded lower than the respective coal baseline measurements. An increase in the production of the lighter hydrocarbon (i.e. CO) from the coal matrix due to the possible exothermic reactions[13], pyrolytic cracking[25] and increased

surface area and pore structure[26], in the near-burner zone is visible from the first set of radial profile measurement at module 1. However, a shift can be seen as the reactions carry forward in the later part of stationary combustion source (module 2, port 2 position) where the concentration of CO starts to reduce in order to facilitate the self-reduction of oxide phases of iron with non-conjectural NOx reduction (Figure 8a). This has been discussed to be linked with the oxides of iron / iron as a gas phase catalyst or as indirect heterogeneous NOx reduction catalyst [20]. There is also evidence associated with the iron metal cations in the ion-exchanged forms, present in coal or coal ash, changing the partitioning of heavy hydrocarbon to lighter hydrocarbon [22].The in furnace reduction of NO achieved without the need of an additional reactor has been reported in literature[20, 22] not only under fuel rich but equivalently in fuel lean conditions.

It can be inferred from the traverse profiles (Figure 8a) that the test facility burner flame is not exactly symmetrical from the center axis of the burner, due to heterogeneous combustion characteristics of coal. The error bars are shown in Figure 8a, also takes into account the 95% accuracy confidence of the data based on the standard deviation. The O_2 trends for the module 1 (port 1) position are relatively at lower level values compared to module 2 (port 2) position, indicative of the extension of fuel-rich combustion zone from the burner quarl up till module 1 position. Figure 8b also indicates a shift from the fuel rich zone to fuel lean zone while moving axially down to the flue emission point. A net 8.2% NO reduction was achieved with 3.5 vol. % Silanite™ injection. It has been reported that the surface to surface based reactions is mainly responsible for the solid iron based additives, however, the gas species might also play a role towards NO destruction in fuel rich zones[20]. Even though the iron oxide chemical redox reactions have a negative Gibbs free energy, the NO destruction

would still converge to a limit (optimum value) as the mass fraction of the additive is increased.

The collected fly ash from the pilot scale facility was subjected to analysis using the scanning electron microscope with energy dispersive spectroscopy. Table 7 summarizes the overall spectrum with 5 no of iteration of the metal % present in the fly ash samples with and without the additive. It is shown that the based on the spectrum analysis the metal concentration of iron in the fly ash increased by about twofold. The results show the net reduction in the K% which is beneficial to suppress the potassium based corrosion sulphidation reactions. The previous tests [12] have shown the formation of the magnetite phase due to the possible interaction of fayalite and CO_2. Moreover, the presence of Fe_2O_3 at 1100^{o}C with the potential formation of magnetite at about 700^{o}C has also been reported by other researchers [22, 27-28].

3.3. **Corrosion test results.** In an industrial application, the fireside corrosion poses a vital challenge so as to reduce the downtime required to fix the failed superheater (SH) and reheat (RH) section boiler tubes. In order to examine the effect of Silanite™ on alloy specimen T22 (widely used for SH and RH boiler section tubes) was tested under simulated flue gas concentration. Figure 9 presents the mass gain and rate of corrosion of the alloy T22 specimens after 1000h exposure at 570^{o}C, coated with coal and Silanite-coal fly ash collected from both the 100kW$_{th}$ and commercial boiler (260tons/h steam production rate).

The Silanite-coal fly ash-coated T22 alloy presented reduced corrosion rates (Figure 9b) compared to the simple coal fly ash-coated and non-coated specimens. Since, the total amount of alkali oxides reported in Table 1, especially the volatile oxides (Na_2O, K_2O) of

the collected Silanite™ + Coal fly ash sample (used for coating purposes) is lower than coal fly ash. This has a direct impact on the known reactions associated with the transformation of alkali chlorides to form alkali sulphates (K_2SO_4) reacting with the oxides of iron (Fe_2O_3) and SO_3, eventually resulting in the formation of alkali iron trisulphates[29-31]. This compound known for its lower melting point dependent fluidity could enhance the rate of corrosion[29] and the steps involved are pictorially explained in Figure 10. The triggering alkali oxides at high temperature react with the water vapours of the surrounding simulating gas mixture to form alkali hydroxide (KOH, NaOH) which after reacting with SO_3 form alkali sulphates (K_2SO_4, Na_2SO_4) deposits. Moreover, the continuous formation of these sulphates allows the diffused oxygen to the metal scale of the specimen to form trioxide of iron (Fe_2O_3) which reacts with SO_3 to form iron sulphates ($Fe_2(SO_4)_3$). The already formed K_2SO_4 would then react with $Fe_2(SO_4)_3$ to form the molten layer of low melting alkali iron trisulphates [29-31]. Eq. 8 summarises these reactions with a rate dependent on the concentration of sulphates of the oxides of alkali.

$$3K_2SO_4 + 3SO_3 + Fe_2O_3 \Leftrightarrow 2K_3Fe(SO_4)_3 \quad [29\text{-}31] \qquad (8)$$

The primitive deposits associated with the sulphates; K_2SO_4, Na_2SO_4 have melting points[32] of 1067ºC, 888ºC respectively. However, the thermal stability limit of the alkali iron trisuphates is around 570ºC - 590ºC [31, 33]. This unstable molten compound reacts with the base metal of the T22 alloy as per the eq. 9 resulting in the loss of the thickness of the boiler tube wall thickness.

$$2K_3Fe(SO_4)_3 + 10Fe \Leftrightarrow 3K_2SO_4 + 3FeS + 3Fe_3O_4 \quad [33\text{-}34] \qquad (9)$$

It has been earlier reported that the formation of the alkali molten complex progresses[33-34] (eq. 9) in the form of a continuous reaction cycle, due to the formation of the K_2SO_4 (eq. 8). In the present study due to the presence of relatively lower concentration of oxides of potassium in the Silanite + Coal fly ash samples (both 100kWth and 260 tons/hr steam producing boiler), the formation of these alkali molten complex would be lower resulting in the evident reduced corrosion rates compared to the coal fly ash samples.

In relation to high temperature, chlorine based fireside corrosion, the direct attack of HCl present in the combustion gaseous products results in $FeCl_2$ formation, which upon oxidation produces Cl_2 able to penetrate directly to the metal resulting in a phenomenon called "metal chlorination at the metal surface"[35] (summarized eq. 10).

$$2Fe + 2HCl + 2FeCl_2 + 3O_2 \Leftrightarrow 2Fe_2O_3 + H_2 + 3Cl_2 \quad [35, 36] \qquad (10)$$

In the presence of the higher concentration of Fe_2O_3 (Table 1) in the Silanite + coal fly ash samples, a protective coating layer could potentially act as a barrier stopping the direct contact of HCl with the base metal (eq. 11). The iron oxide would then react with the HCl / Cl_2 at the deposit coated surface before they could diffuse into the base metal.

$$Fe_2O_3 + 6HCl \rightarrow 2FeCl_3 + 3H_2O \qquad (11)$$

Moreover, the formation of Chromia (Cr_2O_3- present in the Silanite + coal fly ash) approximately twice compared to the coal fly ash could (Table 1) can act as a very protective layer preventing the iron-rich oxides formation of the iron from the base metal[37]. The above explained mechanisms in the presence of the additive can be summarized as

follows: higher alkali oxides and lower oxides of iron concentrations in the deposit formations are expected to lead to higher corrosion rate.

Figure 9a show that the Silanite™ mostly increased the weight gain of the samples, and that the T22 alloy without any coating had the highest weight gain. The pure T22 alloy without any coating due to the direct exposure to the simulated flue gas concentration produced oxidative layers of the oxides of the base metal. The SEM/EDS results of the cross-sectional view of the corroded T22 specimen without any coating (Figure 11a) only indicated rich in Fe, O_2 and Cr in the intact oxide scale compared to the only Fe, Cr and Mo of the base metal. Due to the high presence of Fe and O (Fe_2O_3) along with Cr, the iron oxide can then form a thick layer of $FeCr_2O_4$ (chromium / iron compound spinel) as evident from the EDS of the Figure11a. Similarly, with the presence of additional iron oxide of Silanite™ + Coal fly ash and twice the amount of Chromia (Cr_2O_3), the formation of the same complex Fe/Cr spinel can add to the overall weight gain (Figure 11c). The molar mass of $FeCr_2O_4$ i.e. 223.8 g/mol is also relatively higher compared to the molar mass of oxide of iron i.e. Fe_2O_3: 159 g/mol. In case of the observed findings with the Silanite™ + Coal fly ash coatings, the weight gain due to Fe/Cr spinel formation could exceed the decrease in the weight gain due to the lower corrosion rate. Therefore, in the Figure 9b, an overall weight gain in case of Silanite™+Coal fly ash has been observed. The lower concentration of O (35.8%) in the mapped box (Figure 11c) of the simulated flu gas exposed Silanite™+Coal fly ash coating, compared to the O (52.3%) (Figure 11b) of the Coal fly ash coating especially with lower K (0.3% instead of 0.9%) endorses the presence of lower concentration of the low melting complexes compared to $2K_3Fe(SO_4)_3$. It is also interesting to observe that the thickness of the scale formation due to corrosion above the base metal is slightly thicker in case of the

T22 alloy with and with coal fly ash coating (Figure 11a-b), compared to the Silanite™+ Coal fly ash coating (Figure 11c).

The average surface area of each of the specimen coupon is approximately 1.5cm^2, the mass density gain of the studied samples (g/cm^2) are as follows: T22 without coating = 16.67, T22 Coal fly ash from the 100kWth CTF = 10.23, T22 Silanite+ Coal fly ash from the 100kWth CTF = 10.47, T22 Coal fly ash from the 233MWth boiler = 5.6 and T22 Silanite+Coal fly ash from the 233MWth boiler = 11.37. A similar study[38] on T22 alloy with different coatings produced a higher density gain of 45 mg/cm^2, due to the wide difference between the alkali oxide / sulphates concentrations though with the similar iron oxide concentration.

The coating of the additive does imply positive impact on the corrosion resistance, however, this impact needs to be analysed whether it is significant enough to improve the life span of the real power plant boiler tubes. In the present study with 2.25Cr ferritic steel tubes the minimum and maximum corrosion rates (mm/year) of approximately 0.345 and 0.352 was achieved with Silanite™+Coal fly ash coatings produced from both the pilot and commercial tests. Usually 33% of the thickness is the limit for corrosion in the boiler tubes, which for a typical 38mm diameter superheater tubes is about 1.51mm [39]. The life span of the boiler tubes due to coating can be assumed to be reasonable to estimate from the achieved corrosion rates. Therefore the life span of the corrosion deposit without additive coating will approximately be 1.51/0.468 which equals an estimated value of 3.2 years; whilst the corrosion with additive coating will have a life span of 1.51/0.352 which equals an estimate of 4.2 years. This investigation reveals that the Silanite™ additive is capable of increasing the life span of a high temperature super-heater tubes by approximately 1 year.

4. CONCLUSIONS

The results of the study show that the additive process can benefit lower NOx emissions, lower particulate emissions with improved combustion and that the impact on the effect of deposits on boiler tube can be positive rather than negative. The process has demonstrated at commercial scale that a net 42% reduction in LOI, 20% decrease in the particulate matter of ESP, 8% NOx reduction with 11^{o}C increase in the flame front for 3.5 vol. % Silanite injection can be achieved on a 233MWth (260-280 tons/hr steam output) pulverized fuel boiler. Radial and axial profile measurements from the pilot scale 100kW$_{th}$ furnace also endorsed the reported mechanism of Silanite™ - NO reduction and production of the lighter hydrocarbon. The corrosion study with the additive coated T22 alloy specimens exposed to 560 ^{o}C for 1000hr proved retardation in the corrosion rate. This is acknowledged with the positive affect of the fuel additive due to the presence of relatively lower concentration of oxides of potassium in the Silanite™ + Coal fly ash samples, the formation of molten layer of low melting alkali iron trisulphates complex would be lesser resulting in the evident reduced corrosion rates compared to the coal fly ash samples. Similarly, in the presence of the higher concentration of Fe_2O_3 in the additive- coal fly ash samples, a protective coating layer could potentially act as a barrier stopping the direct contact of HCl with the base metal. Hence, the high iron oxide content with the fewer alkali compounds in the additives abetted to reduce the corrosion rate. This concluded that the fuel additive (Silanite™) did not just improve the boiler combustion efficiency with improvements in particular matter emission, LOI, NOx reduction of the pulverised combustion boiler but also capable of having a positive effect on the fireside corrosion of super-heated boiler tubes.

AUTHOR INFORMATION

Corresponding Author

‡ Dr. Syed Sheraz Daood, Level 1, Arts Tower, Energy Engineering Group, Energy 2050, Department of Mechanical Engineering, University of Sheffield, Sheffield, S10 2TN, UK.

Email: s.daood@sheffield.ac.uk

Author Contributions

The manuscript was written through contributions of all authors. All authors have given approval to the final version of the manuscript. These (‡, †, ††, ‡‡) authors contributed equally.

ACKNOWLEDGMENT

Additive base technology is patented by IIT UK Ltd GB (GB 2516728). The support of analytical team at the International Innovative Technologies UK Ltd and the independent body due diligence experts to monitor the commercial full scale boiler tests is highly appreciated. Authors would also like to thank Mr. Scott Taylor for his in valuable industrial test site support and all other involved research groups. The support from post graduate student (Tom Yelland) and technicians is highly commended. The project has been partly funded by TSB through KTP-008393 and the corrosion results have been funded under the innovation agreement industrial grant (IIT Ltd).

REFERENCES

1. World Nuclear Association website; http://www.world-nuclear.org/information-library/energy-and-the-environment/renewable-energy-and-electricity.aspx.

2. World Coal Association website; http://www.worldcoal.org/file_validate.php?file=Coal%20Facts%202015.pdf.

3. Ouyang, Z.; Zhu, J.G.; Lu, Q.G.; Yao, Y; Liu, J.Z. The effect of limestone on SO_2 and NOx emissions of pulverized coal combustion preheated by circulating fluidized bed. *Fuel* **2014**, *120*, 116–121.

4. Shui-jun, Y.; Feng-cheng X.; Bo-yu, J.; Peng-fei, Z. Influence study of organic and inorganic additive to coal combustion characteristic. *Procedia Environmental Science* **2012**, *12*, 459-467.

5. Technical report on PentoMag® 2550 anti-slagging coal additive. Accessed on 12.02.2016. http://www.pentol.com/sites/default/files/pentomag2550-techinfo.pdf

6. Mortson, M.; Xia, Q. Advanced pollution control-the airborne process and its benefits to china. Accessed on 12.02.2016. http://www.airbornecleanenergy.com/uploads/3/8/7/6/38765463/paper_for_china_conference.pdf

7. Qin, L.; Zhang, Y.; Jan, J.; Chen, W. Influences of waste iron residue on combustion efficiency and polycyclic aromatic hydrocarbons release during coal catalytic combustion. *Aerosol and Air Quality Research* **2015**, *15*, 2720-2729.

8. Gong, X.Z.; Guo, Z.C.; Wang, Z. Variation on anthracite combustion efficiency with CeO_2 and Fe_2O_3 addition by differential thermal analysis (DTA). *Energy* **2010**, *35,* 506–511.

9. Mendiara, T.; Diego, L.F.; Labiano, F.; Gayán, P.; Abad, A.; Adánez, J. On the use of a highly reactive iron ore in chemical looping combustion of different coals. *Fuel* **2014**, *126*, 239–249.

10. Zhang, S.; Chen, Z.; Chen, X.; Gong, X. Effects of ash/K_2CO_3/Fe_2O_3 on ignition temperature and combustion rate of demineralized anthracite. *J. Fuel Chem. Technol.* **2014**, *42*, 166–174.

11. Zou, C.; Wen, L.; Zhang, S.F.; Bai, C.G.; Yin, G.L. Evaluation of catalytic combustion of pulverized coal for use in pulverized coal injection (PCI) and its influence on properties of unburnt chars. *Fuel Process. Technol*. **2014**, *119*, 136–145.

12. Daood, S.S; Ord, G.; Wilkinson, T.; Nimmo, W. Fuel additive technology- NOx reduction, combustion efficiency and fly ash improvement for coal fired power stations. *Fuel*, **2014**, *134*, 293-306.

13. Daood, S.S; Ord, G.; Wilkinson, T.; Nimmo, W. Investigation of the influence of metallic fuel improvers on coal combustion / pyrolysis. *Energy and Fuels*, **2014**, *28*, 1515-1523.

14. Wang, L.; Hustad, J.E.; Skreiberg, O.; Skjevrak, G.; Gronli, M. A critical review on additives to reduce ash related operation problems in biomass combustion applications. *Energy Procedia*, **2012**, *20*,20-29.

15. Daood, S.S.; Javed, M.T.; Rizvi, A.H.; Nimmo, W. Combustion of Pakistani Lignite (thar coal) in a pilot-scale pulverized fuel down-fired combustion test facility. *Energy and Fuels*, **2014**, *28*, 1541-1547.

16. Hussain, T; Simms, N.J.; Nicholl, J.R; Oakey, J.E. Fireside corrosion degradation of HVOF thermal sprayed FeCrAl coating at 700-800^{o}C. *Surface and Coating Technology,* **2015**, *268*, 165-172.

17. Rizvi, T. Fireside corrosion in oxy-fuel environments and the influence of fuel and ash characteristics on corrosion and deposition. Ph.D. Dissertation, University of Leeds, **2014**.

18. Kazagic, A.; Smajevic, I. Experimental investigation of ash behaviour and emissions during combustion of Bosnian coal and biomass. *Energy*, **2007**, 32, 2006-2016.

19. Masia, A.A.T.; Buhre, B.J.; Gupta, R.P.; Wall. T.F. Characterising ash of biomass and waste. *Fuel Processing Technology*, **2007**, 88, 1071-1081.

20. Lissianski, V.V.; Maly, P.M.; Zamansky, V.M. Utilization of iron additives for advance control of NOx emissions from stationary combustion sources. *Ind. Eng. Chem. Res*, **2001**, 40, 3287-3293.

21. Gradon, B.; Lasek, J. Investigations of the reduction of NO to N_2 by reaction with Fe. *Fuel*, **2010**, 89, 3505-3509.

22. Lasek, J. Investigation of the reduction of NO to N_2 by reaction with Fe under fuel-rich and oxidative atmosphere. *Heat Mass Transfer*, **2014**, 50, 933-943.

23. Fenell, P.S.; Hayhurst, A.N. The kinetics of the reduction of NO to N_2 by reaction with particles of Fe. *Proc. Combust. Inst*, **2002**, 29, 2179-2185.

24. Su, Y.; Deng, W.; Shen, H. Catalysis reduction of NO and HCN/ NH_3 during reburning: a short review. **2012**, *Adv Mat Res*, 354–355:365–368.

25. Nozomu, S.; Nobuta, K.; Kimura, T.; Hosokai, S.; Hayashi, J.; Tago, T.; Masuda, T. Production of chemicals by cracking pyrolytic tar from Loy Yang coal over iron oxide catalyst in a steam atmosphere. *Fuel Processing Technology*, **2011**, 92, 771-775.

26. Noichi, H.; Uddin, A.; Sasaoka, E. Steam reforming of naphthalene as model biomass tar over iron-aluminum and iron-zirconium oxide catalyst catalysts. *Fuel Processing Technology*, **2010**, 91, 1609-1616.

27. Fennell, P.S.; Hayhurst, A.N. The kinetics of the reduction of NO to N_2 by reaction with particles of Fe. *Proc Combust Inst*, **2002**, 29, 2179–2185.

28. Lasek, J.; Gradon´, B. Mo_zliwos´ci wykorzystania _zelaza ijego zwia¸zko´w w niekto´rych działaniach na rzecz ochrony s´rodowiska. *Hutnik- Wiadomos´ci Hutnicze*, **2009**, 76, 813–819.

29. Reid, W.T. *External Corrosion and Deposits: boilers and gas turbines*, American Elsevier, New York, 1971.

30. Tomeczek, J. Corrosion modelling of austenitic steel in molten sulphate deposit. *Corrosion Science*, **2007**, 49, 1862-1868.

31. Nelson, W.; Cain, C.J. Corrosion of Superheaters and Reheaters of Pulverized- Coal-Fired Boilers. *Transaction of the ASME*, **1960**, 194-201.

32. Science lab Website; https://www.sciencelab.com/msdsList.php.

33. Spliethoff, H. *Power Generation from Solid Fuels*, Springer- Verlag Berlin Heidelberg: Berlin, Germany, 2010.

34. Ishigai, S. *Steam Power Engineering*. Press Syndicate of the University of Cambridge: Cambridge, UK, 1999.

35. Gaus-Liu, Xiaoyang. *High-Temperature Chlorine Corrosion during Co-Utilisation of Coal with Biomass or Waste*, Institut fur Verfahrenstechnik und Dampfkesselwesen der Universitat Stuttgart: Germany, 2008.

36. Grabke, H.K.; Reese, E.; Spiegel, M. The effects of chlorides, hydrogen chloride, and sulfur dioxide in the oxidation of steels below deposits. *Corrosion Science*, **37**, 1023-1043.

37. Chandra, K.; Kranzmann, A.; Neumann, R.C.; Oder, G.; Rizzo, F. High Temperature Oxidation Behavior of 9-12% Cr Ferritic / Martensitic Steels in a Simulated Dry Oxyfuel Environment. *Oxid Met*, **2015**, 83, 291-316.

38. Dudziak, T.; Hussain, T.; Simms, N.J.; Syed A.U.; Oakey, J.E. Fireside corrosion degradation of ferritic alloys at 600ºC in oxy-fired conditions. *Corrosion Science*, **2014**, 79, 184-191.

39. Mujibur Rahman, M.; Kadir, A.K. Failure analysis of high temperature superheater tube (HTS) of a pulverised coal-fired power station. *Proceedings of Intl. Conf. on Advance Science*, **2011**, 517-522.

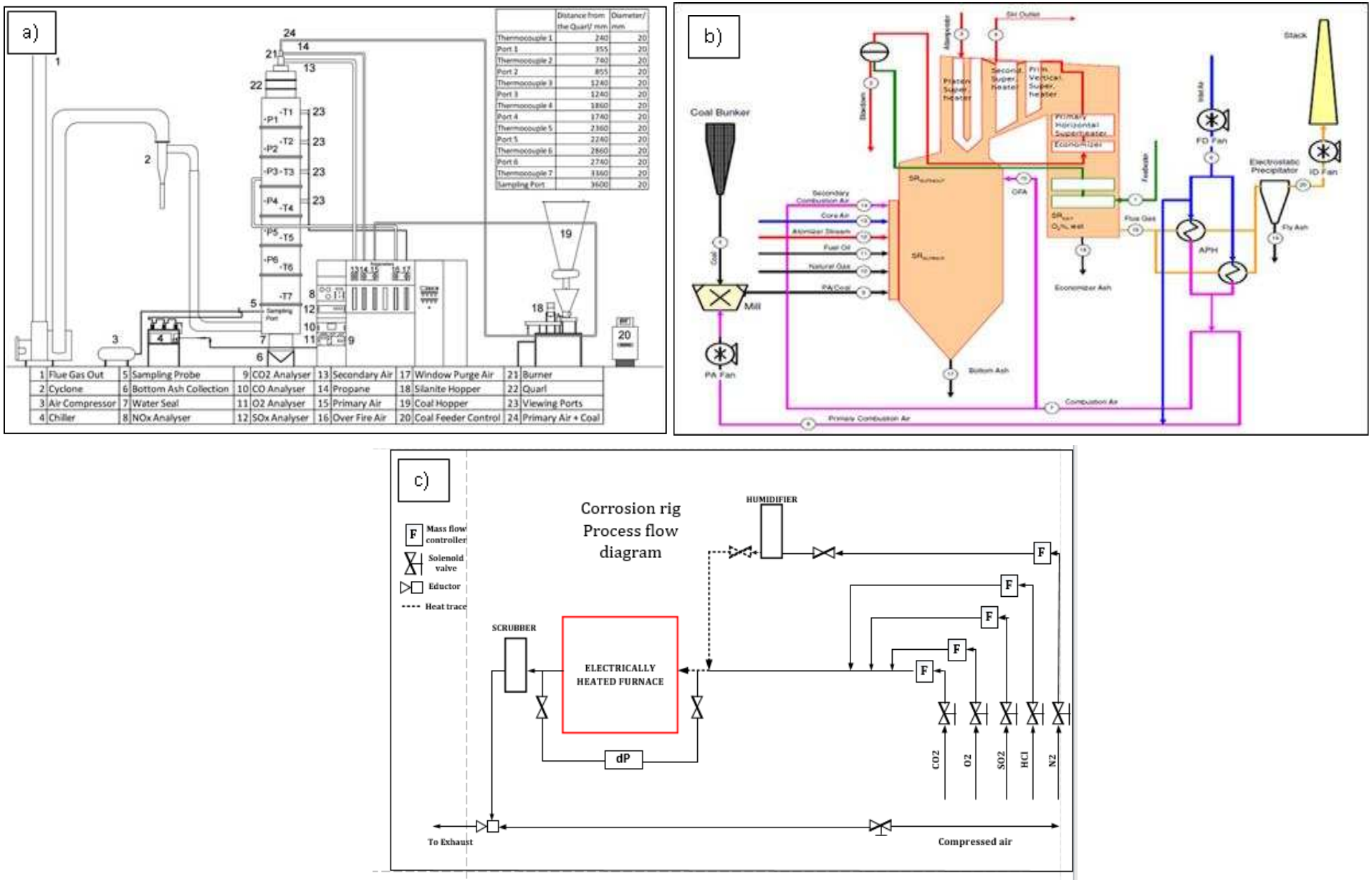

Figure 1. Equipment and schematics of the test facilities: a) 100kW$_{th}$ combustion test facility, b) 260tons/h steam producing commercial boiler, c) simplified schematic of the corrosion test facility

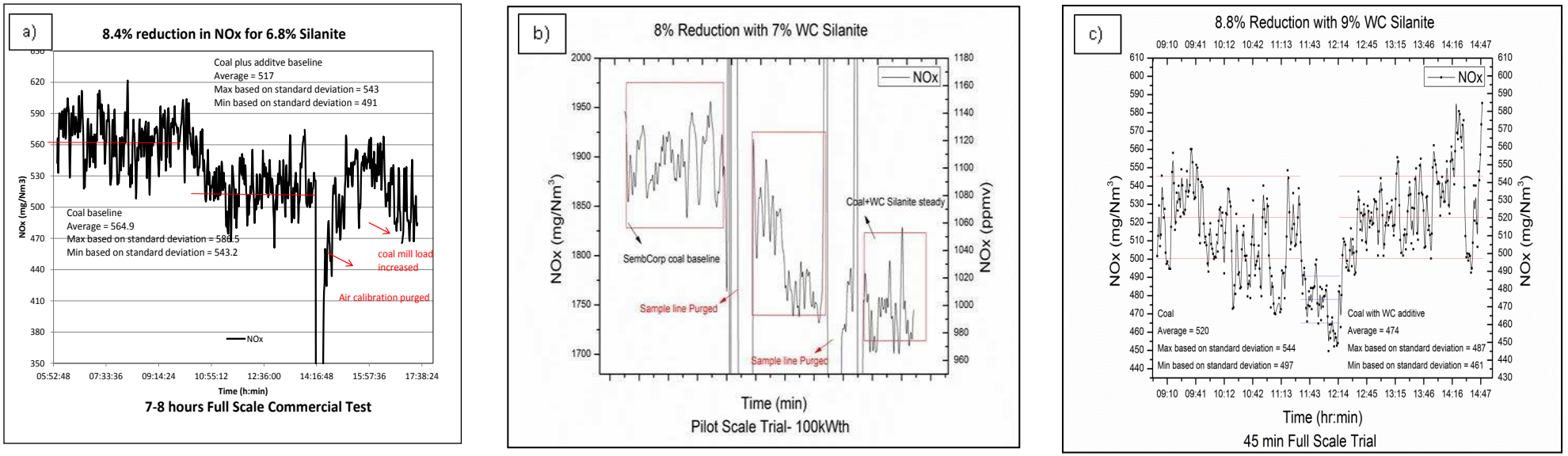

Figure 2. a) NOx profile 8 hours full Scale Commercial Test; b) Pilot Scale Trial- 100 kWth; c) NOx profile 45 min Full Scale Trial[12]

a)

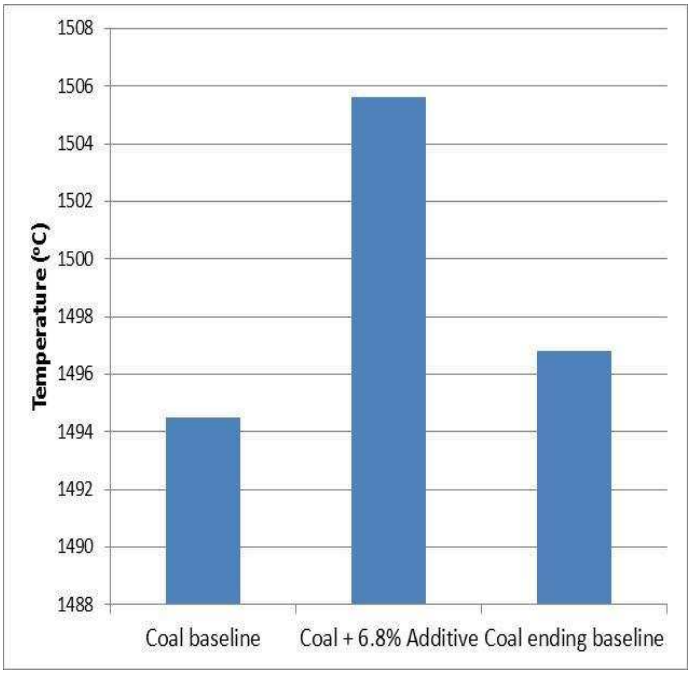

b)

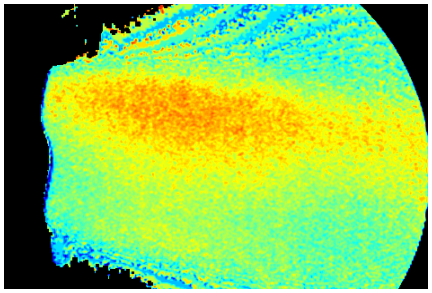

Coal baseline

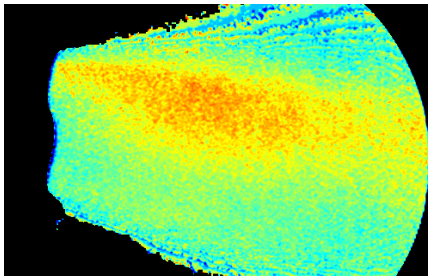

Coal- 6.8% by wt Silanite™

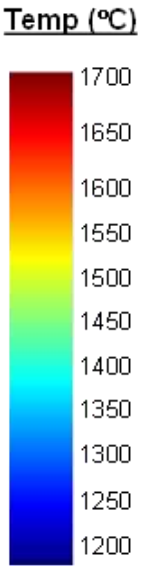

c)

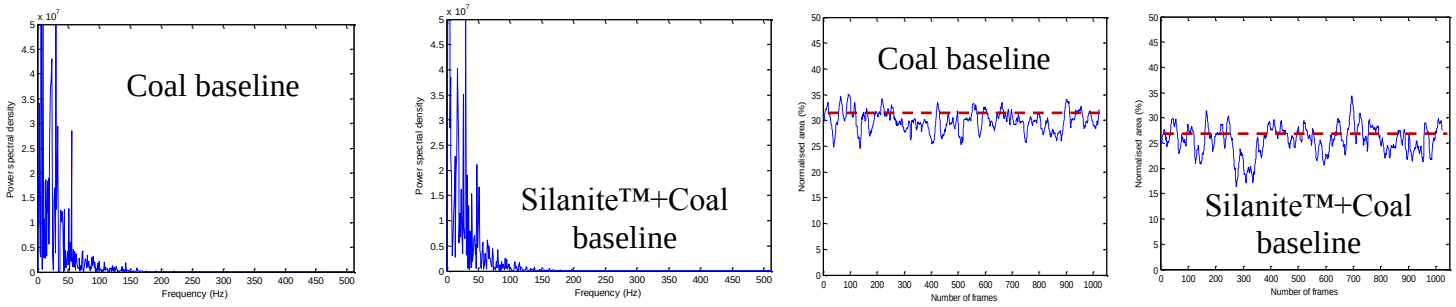

Figure 3. Effect of the injection of Silanite™ on the flame temperature, oscillation frequency and flame area

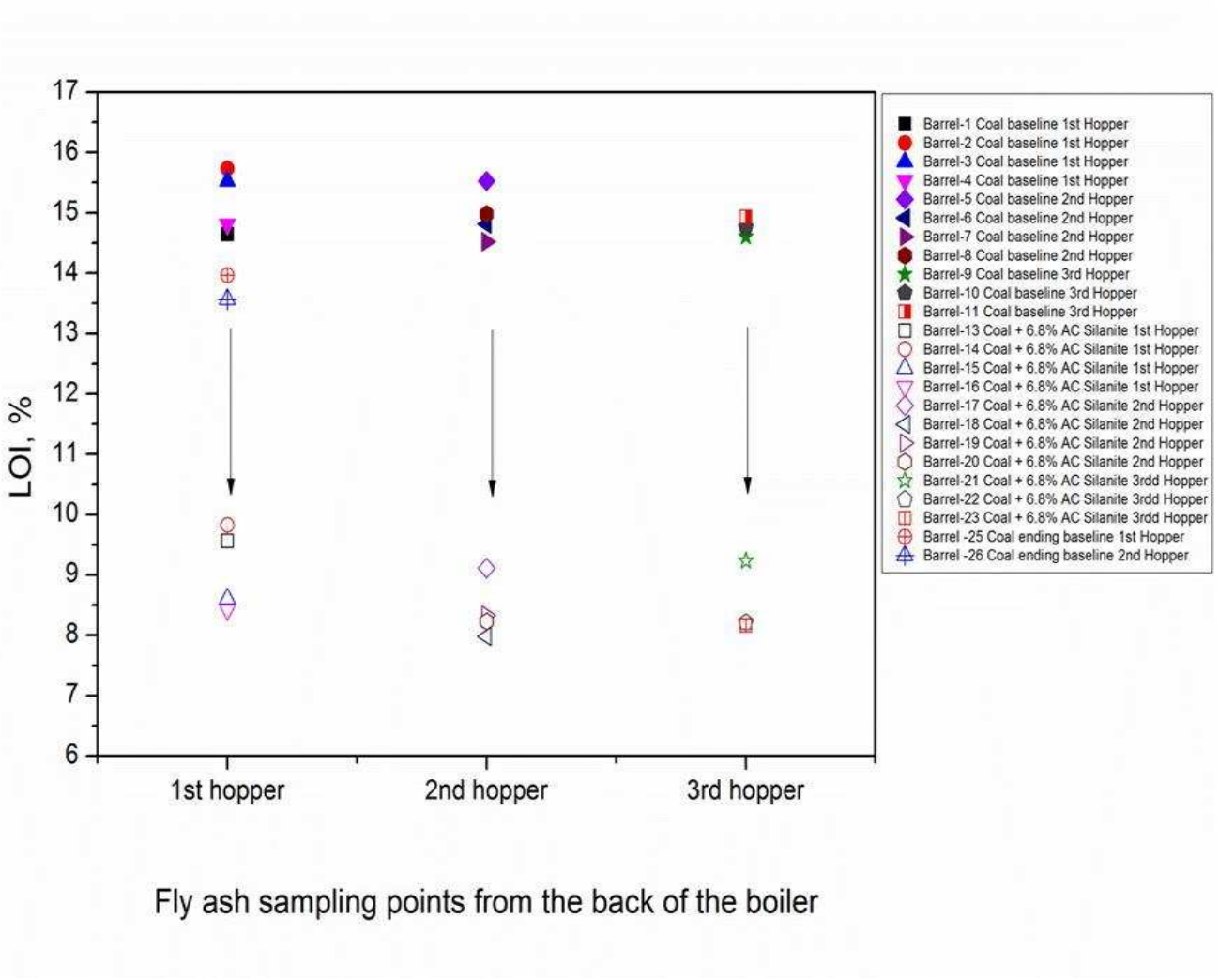

Figure 4. Effect of the injection of Silanite™ on the loss on ignition calculated for collected fly ash samples temperature

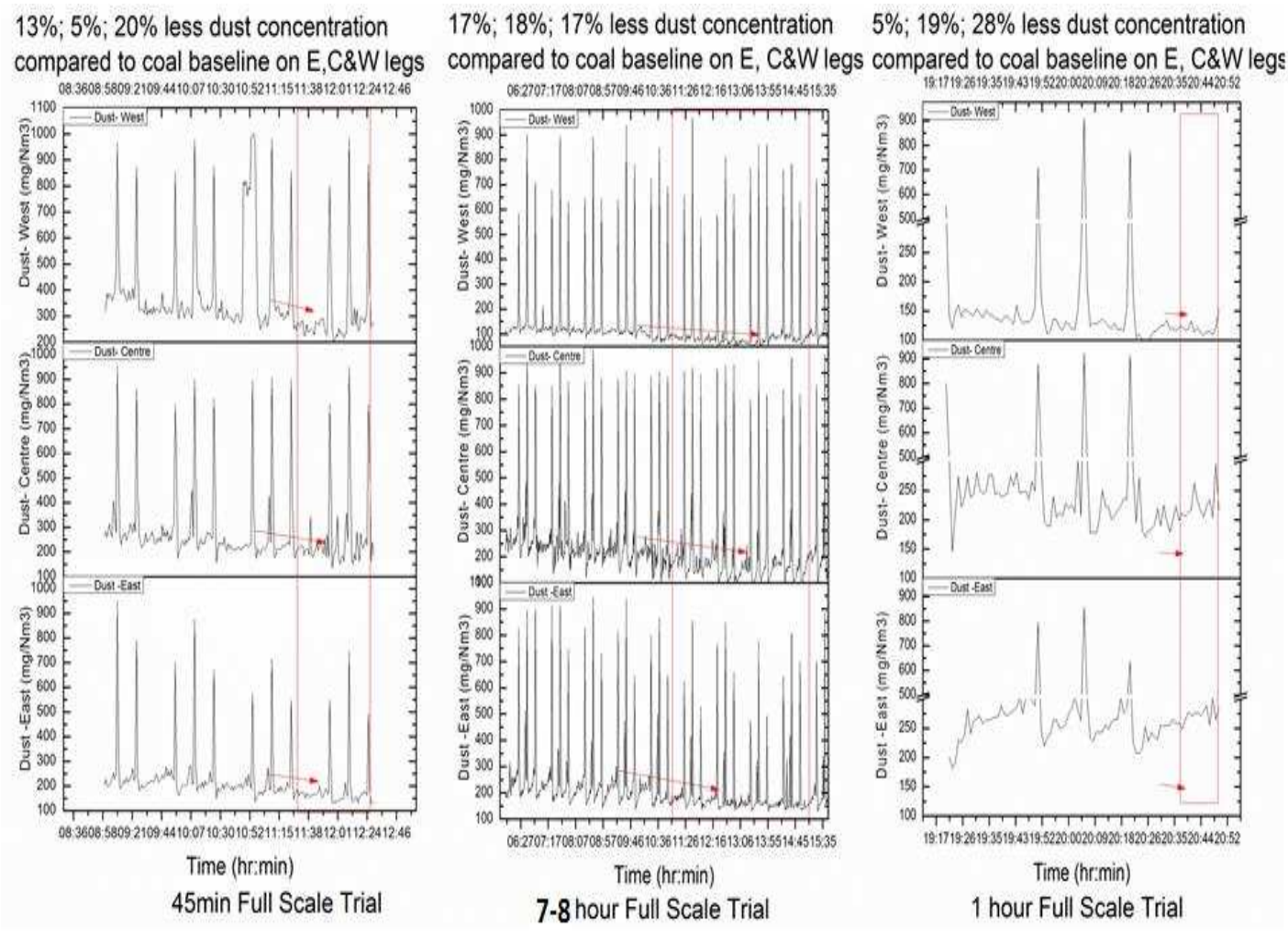

Figure 5. Effect of the injection of Silanite™ on the loss on ignition calculated for collected fly ash samples temperature

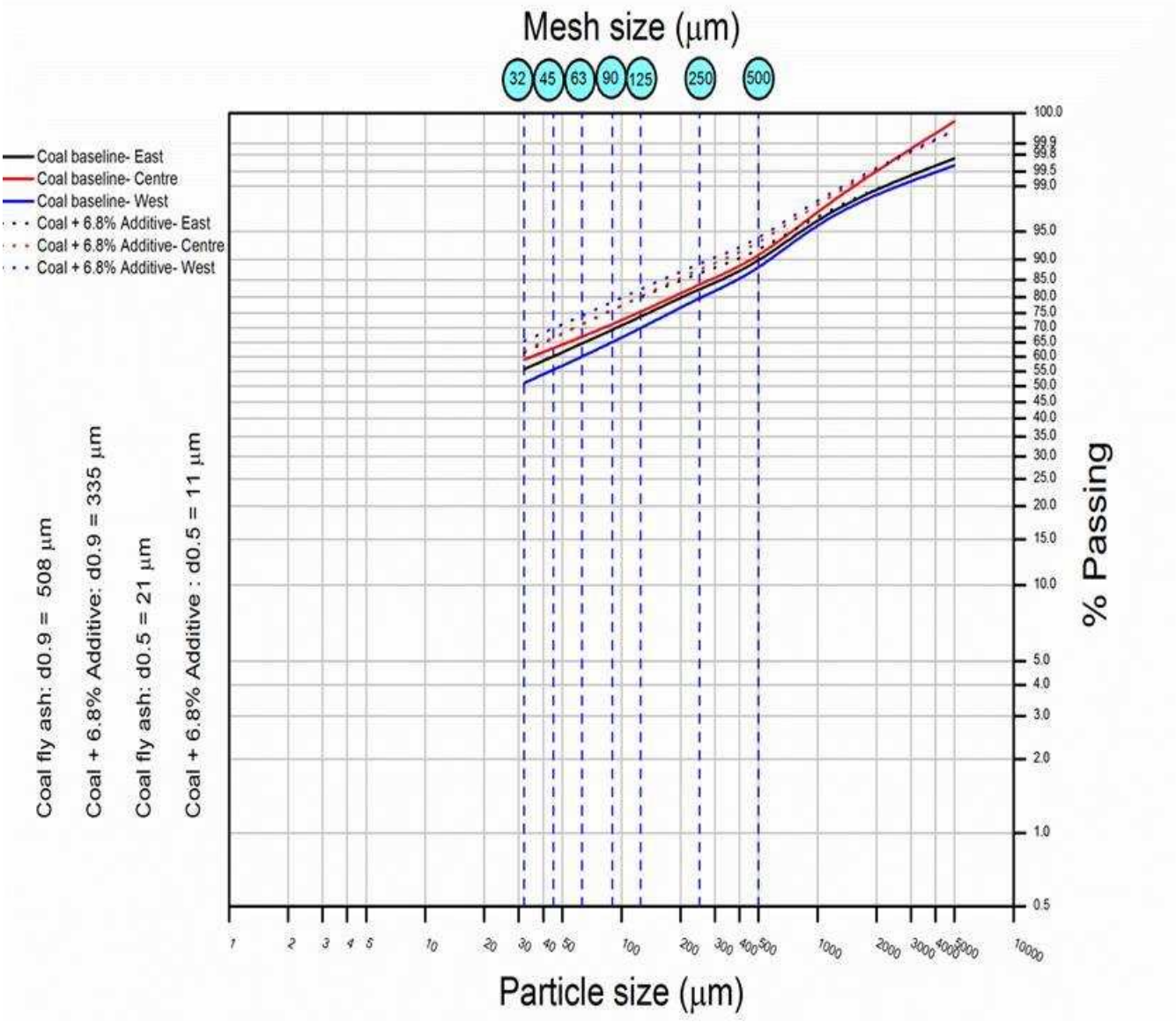

Figure 6. Air jet sieve- Rosin Rammler Distribution with and with Silanite™ injection

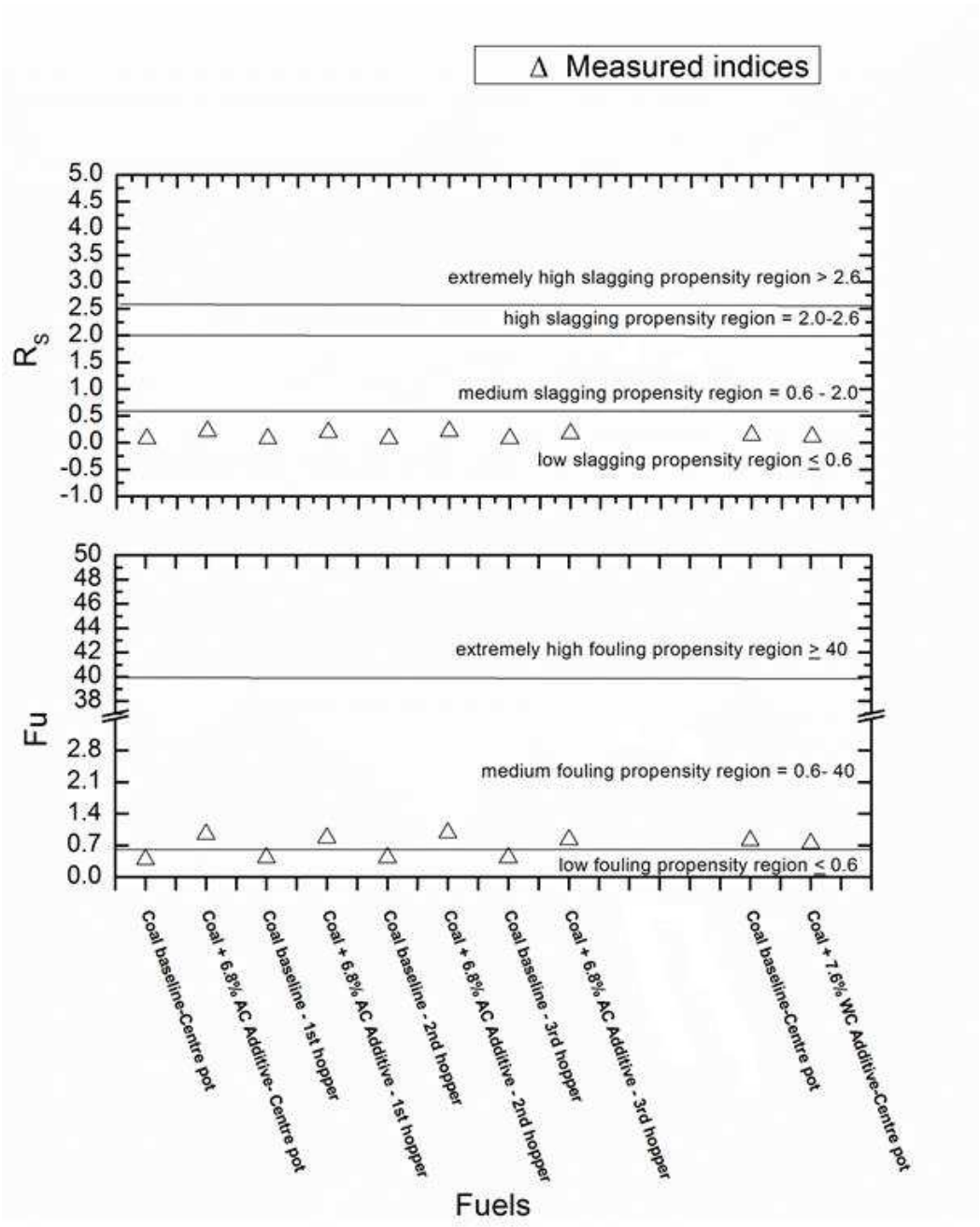

Figure 7. Slagging and fouling indices with and with Silanite™ injection

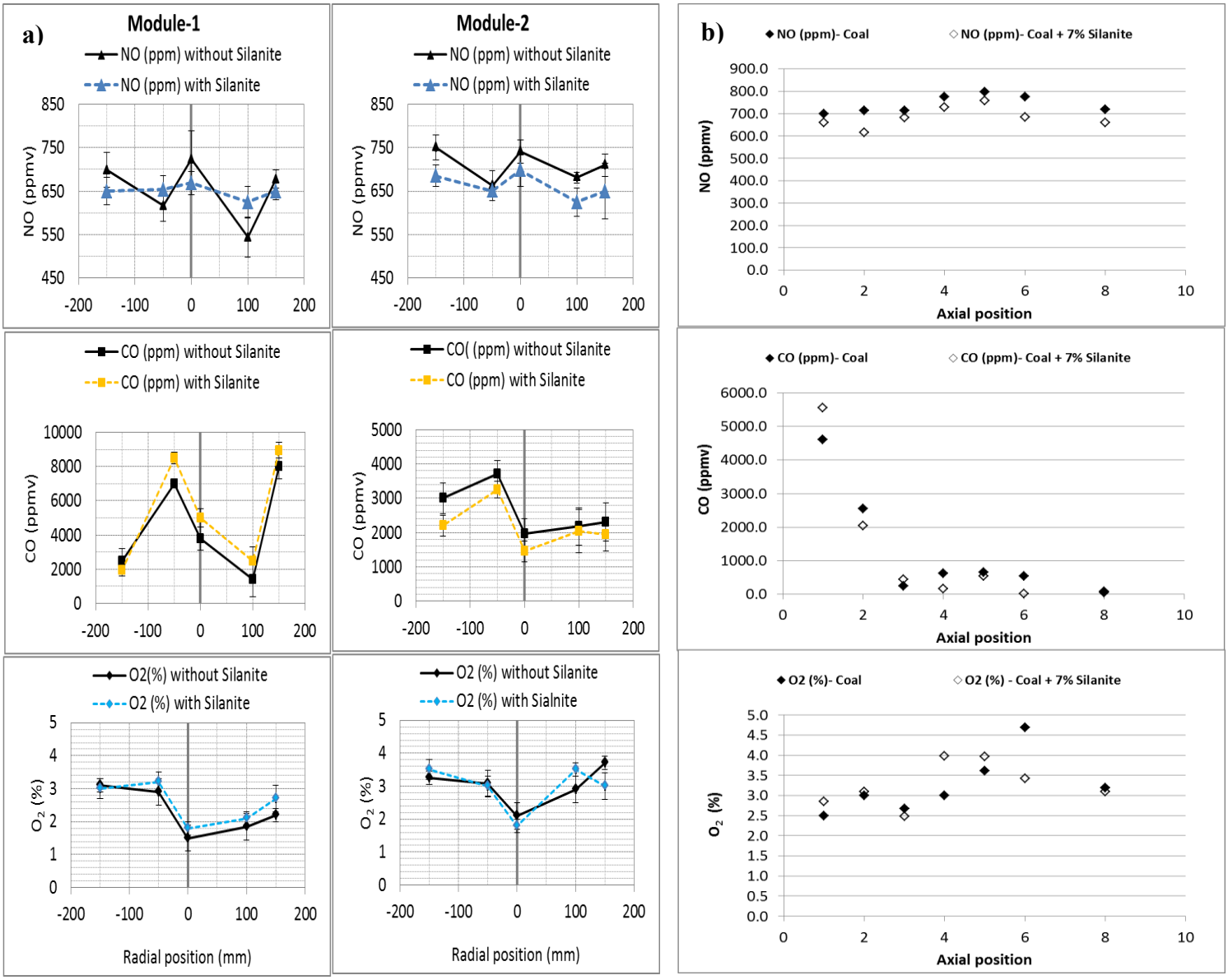

Figure 8. a) Radial profiles with a test sub-bituminous coal imported from outside UK; b) Axial profiles (NO, CO and O_2)

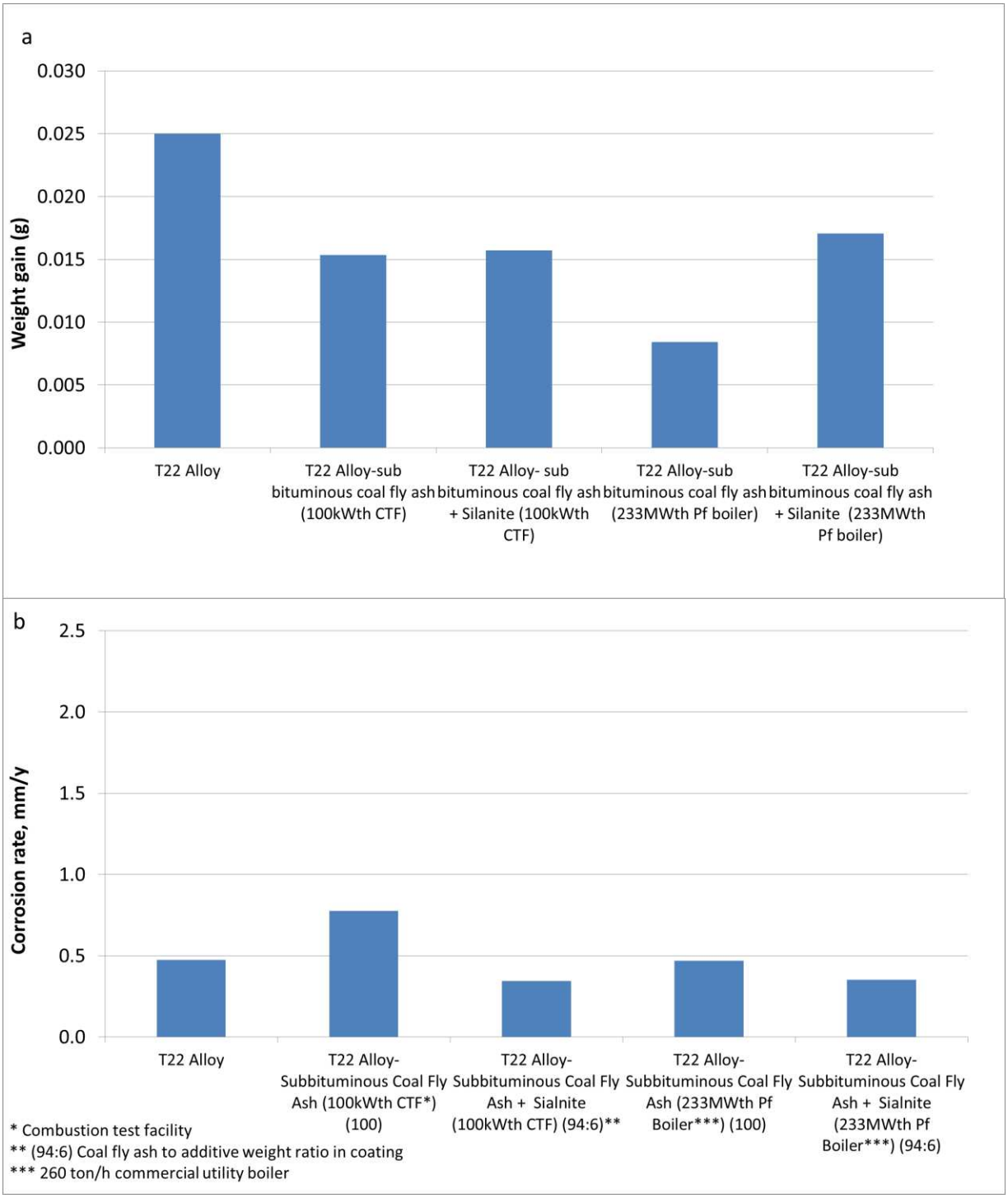

Figure 9. a) Mass gain b) Corrosion rate: after 1000 h exposure of the T22 alloy specimens

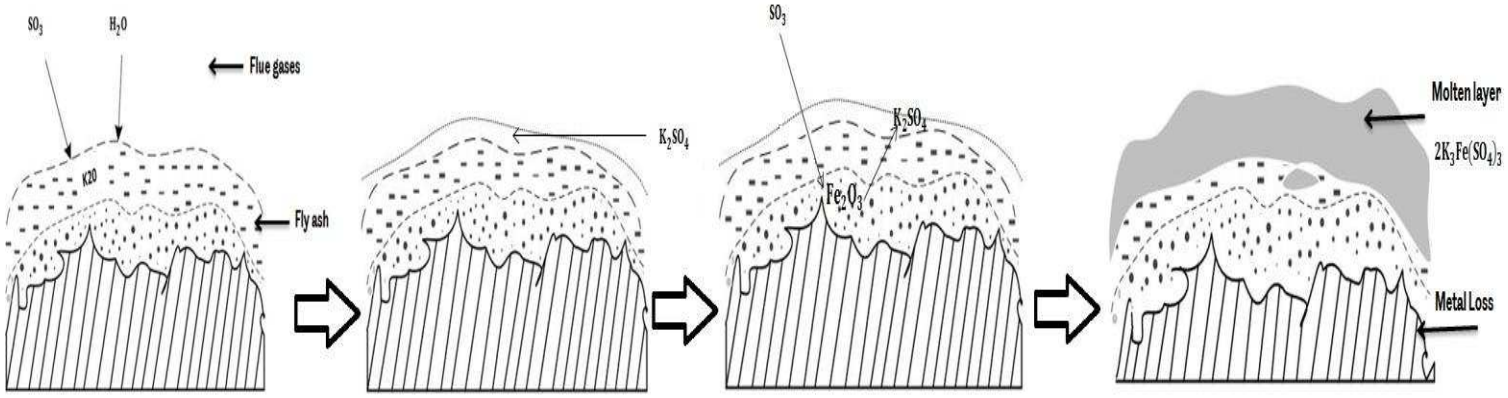

Figure 10. The morphological pictorial representation of the sulphidation reactions

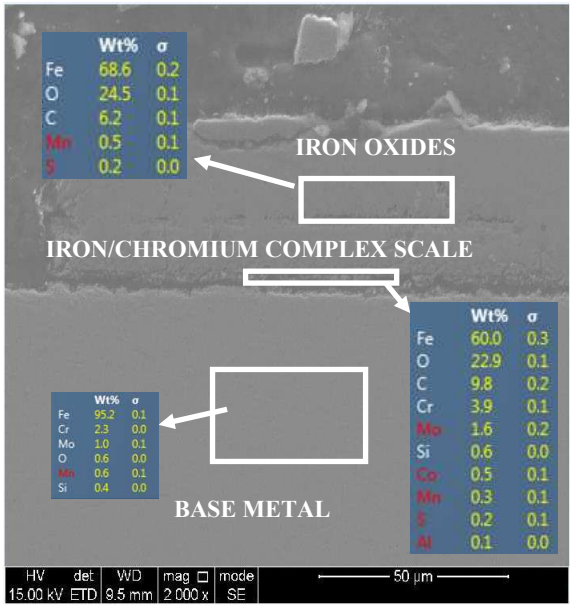

a) SEM/EDS-Cross-section non-coated T22

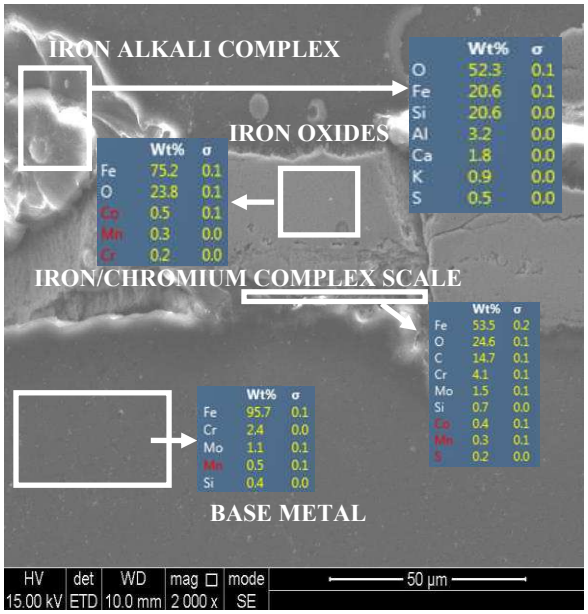

b) SEM/EDS-Cross-section Coal fly ash coated T22

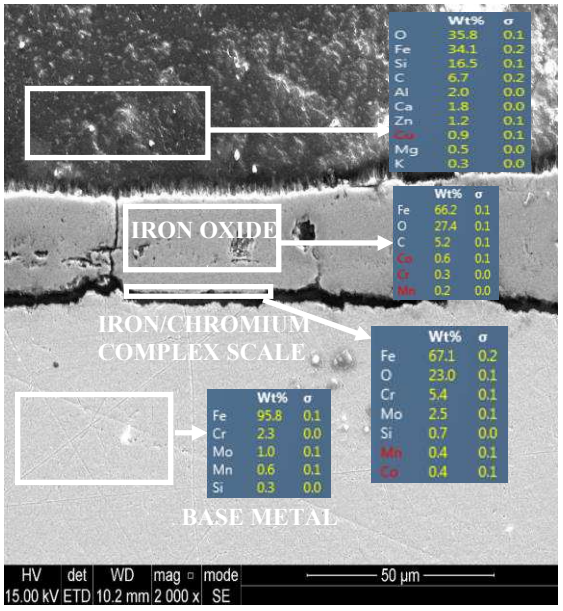

c) SEM/EDS-Cross-section Silanite™ +Coal fly ash coated T22

Figure 11. SEM /EDS of the cross-sectional view of the 1000hr exposure non –coated and coated T22 alloy samples

Table 1. Analysis of Silanite™ and UK-based utility Coal & collected fly ash

Ultimate Analysis as received, %	**UK-Utility Coal**	**Silanite™**
C	66.00	-
H	4.60	
N	2.53	
O (diff)	8.90	
S	0.02	
H_2O	6.00	
Ash	11.95	
Proximate Analysis as received, %	**UK-Utility Coal**	**Silanite™**
Volatile Matter	17.08	-
Fixed Carbon	64.97	-
Ash	11.95	97.5
Moisture	6.00	2.50
Net Calorific Value, MJ/kg	27.04	0
Air Jet Sieving	**UK-Utility Coal**	**Silanite™**
d(0.1) (µm)	11.5	2.5
d(0.50) (µm)	62.5	12
d(0.9) (µm)	181	26
X-Ray fluorescence analysis (% normalized) of the collected fly ash as part of commercial scale test	**UK-Utility Coal fly ash**	**UK- Utility Coal - Silanite™ fly ash**
SiO_2	43.79	37.13
TiO_2	0.81	0.6
Al_2O_3	18.19	14.45
Fe_2O_3	5.15	21.09
MnO	0.04	0.05
MgO	1.63	1.9
CaO	4.91	3.9
Na_2O	0.29	0.46
K_2O	1.7	1.32
P_2O_5	0.45	0.43
SO_3	0.883	0.93
ZnO	0.018	0.34
CuO	0.0087	0.26
PbO	0.0058	0.08
Cr_2O_3	116 µg/g	209 µg/g
LOI + Others	22.12	17.06

Table 2. Timeline based protocol during the test

40.	Soot blowing completion before the test
41.	Coal mill (Babcock type 6.3E9 vertical) 6-A being inoperative due to the maintenance purposes, hence, 6-B and 6-C utilised for maintained coal flows. Coal mill-B load reduced from 12.4t tons/h to 11.38 tons/h from 06:00 to 06:45. Coal mill-C load was reduced from 12.4 tons/h to 12tons/h from 06:00 to 19:19.
42.	Electrostatic precipitators (ESPs) cleaned by ash recovery vacuum system.
43.	Boiler steady load started 07:00 to 10:20.
44.	Blow down left open at ¼ turn on valve, conductivity 16µs (agreed with Parson Brinckerhoff to maintain blow down at ¼ turn throughout the test with or without additive). The blow down flow rate was not measured; its impact on the net change in net boiler efficiency improvement is cancelled for both with and without additive due to consistent ¼ turn opening.
45.	Pf samples taken during the coal steady baseline.
46.	Fly ash recovery system switched off from control room at 07:57
47.	The fly ash hoppers underneath ESPs emptied by ash recovery vacuum system 08:30.
48.	Fly ash and bottom ash samples collection completed by 09:30.
49.	The initial steady base line between 07:00 to 10:10.
50.	Fly ash hopper underneath ESPs by ash recovery vacuum system 10:15.
51.	Additive (3.4% by vol. i.e. 1.59 tons/h) injection started at 10:20. The injection rate was selected in agreement with Sembcorp plant operators and PB's Inspection team.
52.	Pf samples for coal and additive mixture completed 13:20.
53.	Fly ash and bottom ash samples completed by 14:50.
54.	Additive injection stopped at 15:00.
55.	Test concluded at 15:00
56.	The ending baseline was recorded but due to steam demand from customers, coal mills loads were changed resulting in changed ending coal baseline.

Table 3. Net boiler efficiency calculation with and without Silanite™

Calculation of Efficiency of Water tube Boilers with out ADDITIVE											
η (N)B=	$Q_N/Q_{(N)}Z_{tot}$	HEAT OUTPUT									
		Q_N	Useful heat flow (kw)								
η (N)B= Net usefull Boiler Efficiency		mST= is the live steam flow						205	tons/hr	56.96	kg/s
Q(N)= Net heat flow (kW)		mSS= is the spray water mass flow for main steam attemperator						16.2	tons/hr	4.50	kg/s
QN= Useful heat flow (kW)		hFW = is the enthalpy of feed water		Temp.	199.6	deg C	Press.	1841.16	psig	857.24	kj/kg
Ztot= Total Heat input		hST= is the enthalpy of live steam		Temp.	520.6	deg C	Press.	1583.58	psig	3413.81	kj/kg
		hSS= is the enthalpy of spray water upstream of main steam attemperator					Temp.	200.34	deg C	858.14	kj/kg
η =	80.82	QN is calculated as follows					Press.	2136.25	psig		
		QN=	mST(hST-hFW)+mSS(hFW-hSS)								
			145607.59 kW	524.2 GJ/hr							
		HEAT INPUT FROM FUEL									
		$Q_{(N)}ZF$ = mF *[(H(N)+hF)/(1-lU)+μAS*h(N)AS+J(N)A]									
		H(N)tot=	[H(N)+hF]/[1-lu] +J(N)A							27656.76174	kJ/kg
			H(N)= is the NCV of fuel at reference temperature tr=							27043	kJ/kg
			hF= is the enthalpy of fuel = hF=cF(tF-tr)=							-6.18	kJ/kg
				cF= is the specific heat of the fuel=						1.03	kJ/kgK
				tF= is the temperature of fuel=						19.00	oC
				tr= is the temperature of reference=						25.00	oC
			lu=γAsh (1-v)/(1-γAsh - γH2O) [uSL/(1-uSL) ηSL+uFA/(1-uFA) ηFA]							0.024	
				γAsh	Ash content of fuel					0.120	
				γH2O	Water content of fuel					0.060	
				v	Ash Volatile matter,p.37 -EN12952 suggest 0.05					0.050	
		based on 10%unburned combustible in slag		uSL	Unburned combustible content of slag					0.001	
		measured from sample		uFA	Unburned combustible content of fly ash					0.150	
				ηFA	fly ash retention efficiency					0.989	
				mFu= unburned fuel mass flows						0.19	kg/s
				mFo= supplied fuel mass flow				23.39		6.50	kg/s
		based on 1% of ash via coal input		mSL=	Mass of slag					0.008	kg/s
				ηSL	slag collection efficiency	Eq 8.3-41				0.011	
			J(N)A= is the enthalpy of combustion air due to NCV calculation=								
			J(N)A= μA* cpA(tA-tr)							-52.04	kJ/kg
				μA= is the combustion air mass to fuel mass ratio						8.09	
				Combustion air mass flow=				189.16		52.55	kg/s
				Fuel mass flow=				23.39		6.50	kg/s
				cpA= specific heat of air between 25-150oC						1.01	kJ/kgK
				tA= is the air temperature at envelope boundary						18.64	oC
				tr= is the reference temperature						25	oC
			mF= is the fuel mass flow					23.39		6.50	kg/s
		Q(N)ZF= mF* H(N)tot								179681.552	kJ/s
		HEAT CREDIT									
		QNZ= PM+P+QSAE+mAS*h(N)AS		QNZ= is the total heat credit							
		PM= is the Pulverizer power					kW	296.2	measured		
		P =is the power of any other motors					kW	183.2	measured		
		QNZ=	479.402								
		TOTAL HEAT INPUT									
		QNZtot=	QNZF+QNZ								
			180160.95 kW	648.6 GJ/hr							

Calculation of Efficiency of Water tube Boilers with ADDITIVE											
η (N)B=	$Q_N/Q_{(N)}Z_{tot}$	HEAT OUTPUT									
		Q_N	Useful heat flow (kw)								
η (N)B= Net usefull Boiler Efficiency		mST= is the live steam flow						205.385	tons/hr	57.05	kg/s
Q(N)= Net heat flow (kW)		mSS= is the spray water mass flow for main steam attemperator						15.7355	tons/hr	4.37	kg/s
QN= Useful heat flow (kW)		hFW = is the enthalpy of feed water		Temp.	199.2	deg C	press=	1841.17	psig	857.24	kj/kg
Ztot= Total Heat input		hST= is the enthalpy of live steam		Temp.	520.9	deg C	press=	1581.82	psig	3413.81	kj/kg
		hSS= is the enthalpy of spray water upstream of steam attemperator					Temp.	200.62	deg C	858.14	kj/kg
η =	81.87	QN is calculated as follows					Press.	2136.25	psig		
		QN=	mST(hST-hFW)+mSS(hFW-hSS)								
			145851.724 kW	525.1 GJ/hr							
		HEAT INPUT FROM FUEL									
		$Q_{(N)}ZF$ = mF *[(H(N)+hF)/(1-lU)+μAS*h(N)AS+J(N)A]									
		H(N)tot=	[H(N)+hF]/[1-lu] +J(N)A							27346.90356	kJ/kg
			H(N)= is the NCV of fuel at reference temperature tr=							27043	kJ/kg
			hF= is the enthalpy of fuel = hF=cF(tF-tr)=							-6.18	kJ/kg
				cF= is the specific heat of the fuel=						1.03	kJ/kgK
				tF= is the temperature of fuel=						19.00	oC
				tr= is the temperature of reference=						25	oC
			lu=γAsh (1-v)/(1-γAsh - γH2O) [uSL/(1-uSL) ηSL+uFA/(1-uFA) ηFA]							0.013	
				γAsh	Ash content of fuel					0.120	
				γH2O	Water content of fuel					0.060	
				v	Ash Volatile matter,p.37 of EN12952 suggest 0.0					0.050	
		based on 10%unburned combustible in slag		uSL	Unburned combustible content of slag					0.001	
		measured from sample		uFA	Unburned combustible content of fly ash					0.087	
				ηFA	fly ash retention efficiency					0.989	
				mFu= unburned fuel mass flows						0.15	kg/s
				mFo= supplied fuel mass flow				23.39		6.50	kg/s
		based on 1% of ash via coal input		mSL=	Mass of slag					0.008	kg/s
				ηSL	slag collection efficiency	Eq 8.3-41				0.011	
			J(N)A= is the enthalpy of combustion air due to NCV calculation=								
			J(N)A= μA* cpA(tA-tr)							-48.98	kJ/kg
				μA= is the combustion air mass to fuel mass ratio						8.10	
				Combustion air mass flow=				189.33		52.59	kg/s
				Fuel mass flow=				23.39		6.50	kg/s
				cpA= specific heat of air between 25-150oC						1.01	kJ/kgK
				tA= is the air temperature at envelope boundary						19.02	oC
				tr= is the reference temperature						25	oC
			mF= is the fuel mass flow					23.39		6.50	kg/s
		Q(N)ZF= mF* H(N)tot								177665.231	kJ/s
		HEAT CREDIT									
		QNZ= PM+P+QSAE+mAS*h(N)AS		QNZ= is the total heat credit							
		PM= is the Pulverizer power					kW	295.1	measured		
		P =is the power of any other motors					kW	182.9	measured		
		QNZ=	477.965								
		TOTAL HEAT INPUT									
		QNZtot=	QNZF+QNZ								
			178143.1962 kW	641.3 GJ/hr							

Table 4. Dust concentration (mg/Nm3) east-center and west bound legs of the boiler

	Dust particulate-East (mg/Nm^3)	Dust particulates-Centre (mg/Nm^3)	Dust particulates-West (mg/Nm^3)
Coal fly ash	246.3	266.9	148.7
Standard Deviation for coal fly ash calculation	139	158	138
Coal + 6.8% AC Silanite fly ash	206.2	224.5	122.3
Standard Deviation for coal + 6.8% AC Silanite fly ash calculation (-)	133	188	157
Dust reduction w.r.t coal baseline (%)	16.25	15.89	17.76

Table 5. Slagging and fouling indices based on the X-Ray fluorescence (XRF) analysis

Metal in ash reported as %	Sample 7- ESPs coal fly ash 1st Field / 1st hopper	Sample 10- ESPs coal fly ash + 6.8% AC Silanite 1st Field / 1st hopper	Sample 8- ESPs coal fly ash 1st Field / 2nd hopper	Sample 11- ESPs coal fly ash + 6.8% AC Silanite 1st Field / 2nd hopper	Sample 9- ESPs coal fly ash 1st Field / 3rd hopper	Sample 12- ESPs coal fly ash + 6.8% AC Silanite 1st Field / 3rd hopper	Sample 16- Bottom coal fly ash	Sample 17- Bottom coal + 6.8% AC Silanite fly ash
SiO_2	43.25	38.78	43.79	37.13	44.33	39.27	15.42	15.88
TiO_2	0.79	0.63	0.81	0.60	0.81	0.64	0.37	0.39
Al_2O_3	18.24	15.03	18.19	14.45	18.22	15.31	5.80	5.86
Fe_2O_3	5.00	18.92	5.15	21.09	5.09	17.70	3.81	7.24
MnO	0.04	0.05	0.04	0.05	0.04	0.05	0.03	0.02
MgO	1.68	1.38	1.63	1.90	1.67	1.71	0.06	0.07
CaO	4.70	4.13	4.91	3.90	4.86	4.11	3.21	2.85
Na_2O	0.29	0.41	0.29	0.46	0.29	0.41	0.20	0.24
K_2O	1.72	1.39	1.70	1.32	1.70	1.40	0.68	0.65
P_2O_5	0.46	0.42	0.45	0.43	0.47	0.44	0.14	0.18
SO_3	0.9070	0.9790	0.8830	0.93	0.9190	0.92	0.906	1.175
ZnO	0.0192	0.2810	0.0180	0.34	0.0170	0.25	0.009	0.035
CuO	0.0088	0.2239	0.0087	0.26	0.0083	0.20	0.008	0.063
PbO	0.0059	0.0707	0.0058	0.08	0.0051	0.06	0.002	0.008
B/A	0.22	0.48	0.22	0.55	0.21	0.46	0.37	0.50
R(B/A)	0.19	0.45	0.19	0.52	0.19	0.43	0.33	0.47
Rs	0.08	0.19	0.08	0.21	0.08	0.17	0.13	0.23
Fu	0.43	0.87	0.43	0.98	0.43	0.83	0.32	0.44

Table 6. Ash fusibility temperatures

Sample ID	Description	Slagging index calculated on the basis of Deform. Temp and hemi. temp	Ash fusibility temperatures			
		Fs= (4DT + HT)/5	Deformation temperature	Sphere temperature	Hemisphere temperature	Flow temperature
		°C	°C	°C	°C	°C
Sample 7	ESP's coal fly ash 1st field / 1st hopper	1254	1240	1260	1310	1330
Sample 10	ESP's coal fly ash + 6.8% AC Silanite 1st field / 1st hopper	1258	1240	1260	1330	1360
Sample 8	ESP's coal fly ash 1st field / 2nd hopper	1259	1240-1250	1260	1310-1320	1350
Sample 11	ESP's coal fly ash + 6.8% AC Silanite 1st field / 2nd hopper	1258	1240	1260	1330	1360
Sample 9	ESP's coal fly ash 1st field / 3rd hopper	1258	1240	1270	1330	1340
Sample 12	ESP's coal fly ash + 6.8% AC Silanite 1st field / 3rd hopper	1251	1230	1260	1330-1340	1360
Sample 13	AC Silanite	1306	1280	1350	1410	1420
Sample 14	WC Silanite	1342	1320	1390	1430	1440
Sample 19C	Cegrit Pot Coal fly ash 03/04/2014	1270	1260	1260	1310	1330-1340
Sample 20C	Cegrit Pot Coal fly ash + 6.8% AC Silanite 03/04/2014	1252	1240	1250-1260	1300	1340-1350
Sample 21C	Cegrit Pot Coal fly ash 19/05/2014	1252	1240	1260	1300	1340
Sample 22C	Cegrit Pot Coal fly ash + 8% AC Silanite 19/05/2014	1248	1230	1250	1320	1350
Sample 23C	Cegrit Pot Coal fly ash 19/05/2014	1244	1230	1250	1300	1320
Sample 24C	Cegrit Pot Coal fly ash + 8% WC Silanite 19/05/2014	1256	1240	1260	1320	1330

Fs= Slagging index proposed by Gary and Moore

(Gray RJ, Moore GF. Burning the sub-bituminous coals of Montana and Wyoming in large utility boilers. ASME paper; 1974. p. 74-WA/FU-1)

Medium slagging propensity ; 1232 ^{o}C < Fs < 1342 ^{o}C

High slagging propensity; 1052 ^{o}C < Fs < 1232 ^{o}C

Severe high slagging propensity; 1052^{o}C

Table 7. SEM/ EDS of the coal and coal+ Silanite ash

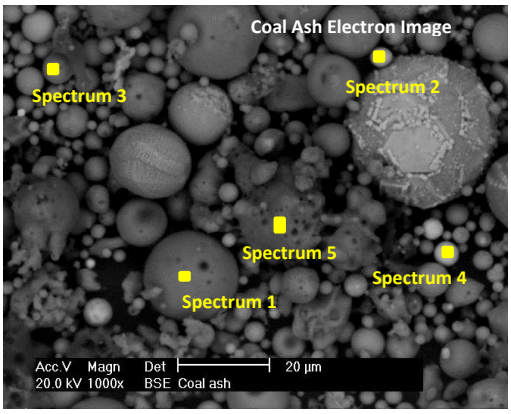

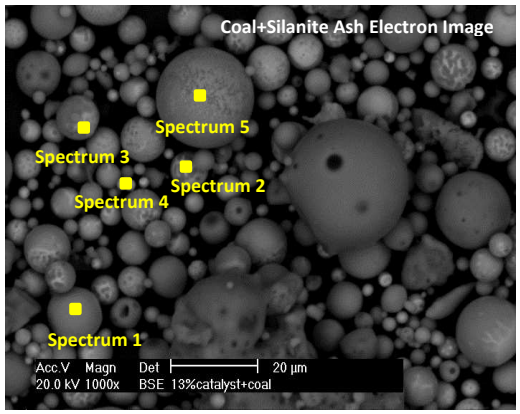

Element Weight %	Coal ash Analysis (normalised spectrum with 5 no of iterations)				
	Spectrum 1	Spectrum 2	Spectrum 3	Spectrum4	Spectrum 5
C K	0.14	3.86	6.36	4.98	53.90
O K	57.00	46.23	58.99	40.80	33.72
Na K	0.58	-	0.62	-	0.18
Mg K	1.13	4.65	0.59	1.00	0.32
Al K	9.91	4.32	11.82	1.61	2.87
Si K	25.62	7.44	18.51	2.61	6.30
K K	2.03	-	1.74	-	0.49
Ca K	1.91	1.67	0.25	6.89	0.78
Ti K	0.34	-	0.36	-	0.20
Fe K	1.61	30.7	0.78	39.51	1.11
P K	-	0.40	-	0.78	-
Mn K	-	0.74	-	1.83	-
S K	-	-	-	-	0.15
Element Weight %	**Coal + 13% Silanite ash Analysis (normalised spectrum with 5 no of iterations)**				
	Spectrum 1	**Spectrum 2**	**Spectrum 3**	**Spectrum4**	**Spectrum 5**
C K	3.66	5.14	10.73	4.50	5.02
O K	46.64	39.43	47.56	53.46	44.51
Na K	0.57	-	0.59	0.77	0.55
Mg K	0.31	0.41	0.40	0.61	0.48
Al K	1.90	1.88	1.90	4.17	1.80
Si K	18.83	13.82	14.01	17.16	16.54
K K	0.41	0.38	0.34	0.83	0.28
Ca K	1.09	1.96	1.22	2.70	1.44
Ti K	-	-	-	0.31	-
Fe K	26.29	36.33	23.25	14.82	29.08
P K	-	-	-	0.36	-
Mn K	-	-	-	-	0.30
S K	-	-	-	0.31	-
Cu K	0.29	0.66	-	-	-